Angular momentum generation in nuclear fission

J.N. Wilson[1], D. Thisse[1], M. Lebois[1], N. Jovančević[1], D. Gjestvang[2], R. Canavan[3,12], M. Rudigier[3,4], D. Étasse[5], R.-B. Gerst[6], L. Gaudefroy[7], E. Adamska[8], P. Adsley[1], A. Algora[9,29], M. Babo[1], K. Belvedere[3], J. Benito[10], G. Benzoni[11], A. Blazhev[6], A. Boso[12], S. Bottoni[11,13], M. Bunce[12], R. Chakma[1], N. Cieplicka-Oryńczak[14], S. Courtin[15,16], M.L. Cortés[17], P. Davies[18],C. Delafosse[1], M. Fallot[19], B. Fornal[14], L. Fraile[10], A. Gottardo[21], V. Guadilla[19], G. Häfner[1,6], K. Hauschild[1], M. Heine[15], C. Henrich[4], I. Homm[4], F. Ibrahim[1], Ł.W. Iskra[11, 14], P. Ivanov[12], S. Jazwari[3, 12], A. Korgul[8], P. Koseoglou[4, 21],T. Kröll[4], T. Kurtukian-Nieto[22], L. Le Meur[19], S. Leoni[11,13], J. Ljungvall[1], A. Lopez-Martens[1], R. Lozeva[1], I. Matea[1], K. Miernik[8], J. Nemer[1], S. Oberstedt[23], W. Paulsen[2], M. Piersa[8], Y. Popovitch[1], C. Porzio[11,13,24], L.Qi[1], D. Ralet[25], P.H. Regan[3,12], K. Rezynkina[26], V. Sánchez-Tembleque[10], S. Siem[2], C. Schmitt[15], P.-A. Söderström[4,27], C. Sürder[4], G. Tocabens[1],V. Vedia[10], D. Verney[1], N. Warr[6], B. Wasilewska[14], J. Wiederhold[4], M. Yavahchova[28], F. Zeiser[2] and S.Ziliani[11,13]

[1]*Université Paris-Saclay, CNRS/IN2P3, IJCLab, 91405 Orsay, France*
[2]*University of Oslo, Department of Physics, P.O. Box 1048, Blindern, 0316 Oslo, Norway*
[3]*Department of Physics, University of Surrey, Guildford GU2 7XH, United Kingdom*
[4]*Technische Universität Darmstadt, Fachbereich Physik, Institut für Kernphysik, 64289 Darmstadt, Germany*
[5]*LPC Caen, 6 Boulevard Maréchal Juin, 14000 Caen, France*
[6]*Institut für Kernphysik, Universität zu Köln, 50937 Köln, Germany*
[7]*CEA/DAM Bruyères-le-Châtel 91297 Arpajon Cedex, France*
[8]*Faculty of Physics, University of Warsaw, PL 02-093 Warsaw, Poland*
[9]*IFIC, CSIC-University of Valencia, Valencia, Spain*
[10]*Grupo de Fisica Nuclear & IPARCOS, Universidad Complutense de Madrid, CEI Moncloa, 28040 Madrid, Spain*
[11]*INFN sez.\ Milano, Via Celoria 16, 20133 Milano, Italy*
[12]*National Physical Laboratory, Hampton Road, Teddington, Middlesex TW11 0LW, United Kingdom*
[13]*Dipartimento di Fisica, Universitá degli Studi di Milano, Via Celoria 16, 20133 Milano, Italy*
[14]*Institute of Nuclear Physics, Polish Academy of Sciences, PL-31342 Krakow, Poland*
[15]*IPHC, 23 rue du Loess, 67037 Strasbourg, France*
[16]*CNRS, UMR7178, 67037 Strasbourg, France*
[17]*RIKEN Nishina Center, 2-1 Hirosawa, Wako, Saitama 351-0198, Japan*
[18]*School of Physics and Astronomy, University of Manchester, Oxford Road, Manchester M13 9PL, United Kingdom*
[19]*Subatech, IMT-Atlantique, Université de Nantes, CNRS-IN2P3, F-44307 Nantes, France*
[20]*INFN Laboratori Nazionali di Legnaro, Viale dell'Universitá, 2, I-35020 Legnaro, Italy*
[21]*GSI Helmoltzzentrum für Schwerionenforschung GmbH, Planckstr.1, 64291 Darmstadt, Germany*
[22]*CENBG, UMR5797, Université de Bordeaux, CNRS, F-33170 Gradignan, France*
[23]*European Commission, Joint Research Centre, Directorate G for Nuclear Safety and Security, Unit G.2, 2440 Geel, Belgium*
[24]*TRIUMF, 4004 Wesbrook Mall, Vancouver, BC V6T 2A3, Canada*
[25]*Grand Accélérateur National d'Ions Lourds, Bd Henri Becquerel, 14076 Caen, France*

[26]*Institute for Nuclear and Radiation Physics, KU Leuven, 3000 Leuven, Belgium*
[27]*Extreme Light Infrastructure-Nuclear Physics (ELI-NP)/Horia Hulubei National Institute for Physics and Nuclear Engineering (IFIN-HH), Strada Reactorului 30, 077125 Bucharest-Măgurele, Romania*
[28]*Institute for Nuclear Research and Nuclear Energy, Bulgarian Academy of Sciences, 1784 Sofia, Bulgaria*
[29]*Institute for Nuclear Research (Atomki), H-4001 Debrecen, Hungary*

When a heavy atomic nucleus fissions, the resulting fragments are observed to emerge spinning[1]; this phenomenon has been an outstanding mystery in nuclear physics for over 40 years[2,3]. The internal generation of around 6-7 units of angular momentum in each fragment is particularly puzzling for systems which start with zero, or almost zero, spin. There are currently no experimental observations which enable decisive discrimination between the many competing theories for the angular momentum generation mechanism[4-12]. Nevertheless, the present consensus is that excitation of collective vibrational modes generate the intrinsic spin before the nucleus splits (pre-scission).

Here we show that there is no significant correlation between the spins in fragment partners, which leads us to conclude that angular momentum in fission is actually generated *after* the nucleus splits (post-scission). We present comprehensive data showing that average spin is strongly mass dependent, varying in saw-tooth distributions. We observe no significant dependence of fragment spin on the mass or charge of the partner nucleus, confirming the uncorrelated, post-scission nature of the spin mechanism. To explain these observations, we propose that collective motion of nucleons in the ruptured neck of the fissioning system generates two independent torques, analogous to the snapping of an elastic band. A parametrisation based on occupation of angular momentum states according to statistical theory well-describes the full range of experimental data. This new information on the role of spin in nuclear fission is not only important for the fundamental understanding and theoretical description of fission, but also has consequences for the γ-ray heating problem in nuclear reactors[13,14], for the study of the structure of neutron-rich isotopes[15,16], and for the synthesis and stability of super-heavy elements[17,18].

The stability of heavy atomic nuclei is governed by a delicate balance between the Coulomb repulsion of the protons which attempt to deform the nucleus, the nuclear surface tension which drives towards spherical configurations, and quantum shell effects which add extra stability for certain nuclear shapes. Fission occurs when there is a perturbation of this balance in favour of the Coulomb repulsion. It is an exothermic, dynamical process that begins as instability in the nuclear shape, which after passing the point of no-return (saddle point) becomes more and more elongated. The nascent fragments form a neck as they move rapidly apart, which quickly snaps (scission). Shell effects in the nascent fragments give rise to certain favoured mass splits, which for low energy fission of actinide nuclei (typically containing ~240 nucleons) produces a light fragment of mass $A \sim 100$ and a heavy fragment of mass $A \sim 140$. Post scission, the decay of each excited fragment is a statistical process. It initially proceeds through efficient removal of excitation energy via emission of typically 0 - 2 neutrons and 1 - 3 high-energy γ rays. Subsequently, the emission of several more γ rays, which usually carry away two units of angular momentum each, removes the majority of the angular momentum and the remaining excitation energy. This prompt de-excitation process ends at the fragment ground states usually within a few nanoseconds[19].

There are many competing theories of how a fissioning nucleus generates its intrinsic angular momentum, and where in the above sequence of events it occurs. One class of explanations proposes that it arises from the excitation of collective vibrational modes such as bending, wriggling, tilting and twisting of the system before it splits (pre-scission). These theories suggest the vibrations are either initiated by thermal excitations[4-6] , arise from quantum fluctuations[7,8], or both together[9]. Post-scission theories suggest that the angular momenta are generated either from Coulomb forces[10] or from deformed fragments which have coupled orientations[11,12]. Since the angular momentum is quickly carried away by the γ rays, the experimental study of the generation mechanism necessarily involves detailed observation of the prompt γ-ray emission.

Experimental attempts to understand the intrinsic spin generation started with low-resolution detection of prompt fission γ-rays in correlation with fragment mass[20,21], which revealed saw-tooth shapes in the γ-ray yields which are strongly related to spin. The major difficulty was the separation of γ rays emitted from the two fragments, and the existence of these patterns was called into question in a later experiment where no saw-tooth was observed[22]. Another experimental approach involves spectroscopy of isomeric (long lived) excited states found in certain nuclei. Measurements of isomer population are highly sensitive to small relative changes in spin. However, only a small subset of all the isotopes produced in fission have such isomeric states and it is difficult to measure trends over a large range in mass[23]. In this present work, we use a third technique[24] based on high-resolution spectroscopy which allows both separation of γ rays from the two fragments and the study of trends over a large mass ranges.

To probe intrinsic generation of angular momentum also requires systems with initial spin of zero or almost zero, namely spontaneous fission or neutron-induced fission. Heavy-ion or charged-particle-induced fission reactions are unsuitable since they generate high initial angular momenta[25], which can obscure the origin of the intrinsic spin.

We present unique and extensive experimental data obtained from fission experiments carried out at the ALTO facility of IJC Laboratory in Orsay with the LICORNE directional, neutron source[26,27] coupled to the high-performance ν-Ball γ-ray spectrometer[28]. We carried out high-resolution spectroscopy of fast-neutron-induced fission of ^{232}Th and ^{238}U, and the spontaneous fission of ^{252}Cf with the addition of an ionisation chamber[29].

Results

For each of the three systems studied we identified characteristic γ-ray decay patterns of excited states in around 30 even-even nuclei (with even numbers of both protons and neutrons). For each even-even fission fragment we extracted the average spin after neutron emission using a method developed at the University of Manchester[24] which combines all the available γ-ray transition intensity and coincidence information (see methods).

Our results (Fig. 1) definitively confirm that fragment spins vary strongly as a function of fragment mass in saw-tooth distributions, similar to the patterns previously observed in γ-ray yields[20,21]. We note that a given fragment spin appears to depend only on the fragment mass, with no significant relationship to the mass of the system which emits it nor the mass or charge of the partner nucleus with which it emerged. This observation does therefore not support theoretical explanations based on post-scission Coulomb effects[10], where a dependence of spin on the product of the fragment charges, Z_1Z_2, would be expected.

Additionally, large asymmetries in average spin are observed for certain fragment pair combinations (e.g. ^{86}Se and ^{150}Ce from ^{238}U(n,f)), where the spin of the heavy fragment can be more than double that of its light partner. The existence of such asymmetries does not support the post-scission explanation based on coupled orientations of deformed fragments[11,12], which explicitly predicts spins of equal magnitudes. Indeed, the existence of such large spin asymmetries provokes the question of how spin generation could possibly occur pre-scission if the fragments are in contact and participating in a correlated collective motion. In that case expected fragment spins at scission would be +*I* and –*I* units. To investigate further, we studied the correlation between spins of the most strongly populated fragments in the $^{238}U(n,f)$ reaction. For a given nucleus, γ-ray transitions of increasing spin were selected from its partner, constraining the partner population to higher and higher spins. We then examined how the average spin of the given nucleus evolved in response (Fig. 2). For example, the most strongly populated partner nucleus of ^{96}Sr is ^{140}Xe. By demanding observation of a γ ray emitted from the lowest 8^+ state in ^{140}Xe we constrain this nucleus to be populated with average spins higher than 8 units of angular momentum. The corresponding average spin in ^{96}Sr is deduced by measuring the corresponding coincident γ ray intensities. By varying the spin conditions and the isotopes studied, we obtain the fragment spin correlations.

The observed slopes are clearly consistent with zero, suggesting an uncorrelated, post-scission spin generation mechanism. The data do not support pre-scission theoretical explanations[4-9] confirming what was suspected from the large spin asymmetries (Fig. 1). It appears that each fragment has no knowledge of the spin generated in its partner.

This unexpected conclusion may resolve the historical controversy surrounding previous experimental results[20,21,22]. For fragment spins which are generated independently, the event-by-event correlations measured in[22] would not be expected to generate a saw-tooth pattern. Hence this absence of saw-tooth may support rather than contradict our current findings.

Discussion

A post-scission, uncorrelated origin of angular momentum suggests that the fragments have become two separate, independent quantal systems. This can be viewed from both macroscopic and statistical/single-particle points of view.

Post-scission generation of two independent torques Macroscopically, we suggest that fragments acquire their spin in a process analogous to the snapping of an elastic band. A neck forms between the two emerging fragments which undergoes first a stretching, then a rupture and finally a relaxation during which the potential energy from the deformed neck (i.e. elastic) transforms into kinetic energy. For asymmetric fission of the actinide nuclei we assume a double cluster, with the cores of the nascent fragments lying near doubly-closed shells and the remaining nucleons from the neck shared between them after rupture (Fig. 3).

We suggest that the nucleons from both halves of the ruptured neck drive the generation of angular momentum in each fragment. The relative sizes of torques will depend on the number of neck nucleons and thus the precise location of the neck rupture, i.e. the configuration at scission. Classically, the neck would rupture in the middle at its weakest point. However, in the subatomic world a gap can appear at any point[30], with decreasing probabilities for more extreme partitions. We suggest that how the system arrives at a specific scission configuration will not have any subsequent impact on the generation of post-scission spin and that the fragments retain no memory of their formation after scission.

At scission the former neck nucleons are located far from the centre of masses of the newly-born fragments in two very elongated configurations. Such extreme elongations have large surface energies which provide the restoring forces towards more spherical shapes. Fluctuations in the aggregate direction of motion of these former neck nucleons generate the two independent torques. Small angular deviations from the fission axis of the collective nucleon motion must occur due to Heisenberg's uncertainty principle for spin/orientation of a system[31]. Uncertainties in the direction of the resulting linear momentum, along the fission axis will result in small perpendicular components that will generate a distribution of angular momenta. Angular momenta in both fragments will point in a plane perpendicular to the fission axis consistent with previous experiements[1], although there will be no correlation or constraint on their relative orientations. The resulting orbital angular momentum, $\vec{\boldsymbol{I}}_{\boldsymbol{o}}$, of the fragments with respect to each other, generated by the components of the motion perpendicular to the fission axis, assures the conservation of the total angular momentum $\vec{\boldsymbol{I}}_{\mathbf{1}} + \vec{\boldsymbol{I}}_{\mathbf{2}} + \vec{\boldsymbol{I}}_{\boldsymbol{o}} = 0$.

The dramatic fragment shape change from elongated to more spherical shapes will also generate heat as the surface energy converts into internal excitation energy, setting the stage for subsequent evaporation of neutrons. Angular momentum, excitation energy and emitted neutron multiplicity will thus be strongly correlated with each other. Indeed, similar saw-tooth distributions are known to occur in average neutron multiplicities as a function of fragment mass[32,33].

Comparison of the variation in average spins to that expected from statistical theory In the statistical/single-particle view, if the newly-formed fragments are independent, then their excited states would be expected to have an angular momentum occupation entirely according to statistical theory. For an excited nucleus, the probability distribution, $P(I)$, of angular momenta, I, was first derived by Hans Bethe[34] and is expected to be:

$$P(I|\sigma^2) = \frac{2I+1}{2\sigma^2}\exp\left(-\frac{(I+½)^2}{2\sigma^2}\right)$$

where σ is known as a spin-cutoff parameter describing the width of this distribution and is directly related to the average spin value, $\langle I \rangle \approx 1.15\sigma$. From statistical theory (see methods) we derive a smooth parametrisation which can be tested for compatibility with our average spin data (Fig. 1):

$$\langle I \rangle = cA_N^{1/4}A_F^{7/12}$$

where c, is a constant and the only free fit parameter, A_F is the fragment mass, and A_N is the mass of neck nucleons. For light and heavy fragments we use values of $A_N = (A_F - 78)$ and $A_N = (A_F - 130)$ near the doubly-magic Ni and Sn shell closures. The derivation presented here has limitations and is not intended as a full description, but as an illustration of the idea (see methods). An extended theoretical description would involve more complex dependencies of the parameters due to structure effects.

Six independent fits using the above parametrisation for each light and heavy peak in the three different systems were performed. The fitted constants are remarkably similar, with a mean of $c = 0.196$ and standard deviation of $\sigma_c = 0.009$, a relative variation of only ~ 4% suggesting that the fragment spins fall on a universal curve. This simple parametrisation thus appears to capture the main ingredients of the spin-mass relationship. We conclude that the experimentally observed variation in the average spins is thus consistent with what is expected from statistical theory for a post-scission, uncorrelated, spin generation mechanism. There may be other second order effects (e.g. Coulomb forces) that are not yet accounted for, but these are clearly small.

A concise suggestion for the mechanism of intrinsic angular momentum generation in the light of our new data is as follows, although we recognise that other interpretations may also be possible:

A fissioning nucleus which starts with zero or near-zero spin undergoes: (i) an unstoppable shape instability from Coulomb forces; (ii) a neck formation between the two emerging fragment clusters; (iii) a neck stretching and rupture (scission) with the birth of two deformed, newly-independent quantal systems; (iv) a shape relaxation of each fragment as surface potential energy converts to excitation of the internal nucleonic degrees of freedom; (v) a resulting occupation of different angular momentum states occurring entirely according to statistical theory for two independent excited nuclei.

In the equivalent macroscopic picture, the last two steps can also be seen as: (iv) a shape relaxation where aggregate collective motions of the nucleons have off-axis components generating two independent torques; (v) the statistical distributions of torques creates two independent distributions of spins.

Consequences

Understanding the angular momentum generated in fission is important for fundamental reasons, but also has consequences for other fields. In nuclear energy applications, fragment spin is related to reactor γ-ray heating effects[13,14], either through the number of prompt γ rays that transport it during reactor operation, or the delayed γ rays from isomeric states which contribute to the decay heat after reactor shutdown. For these reasons many recent measurements of prompt γ-ray characteristics such as average multiplicity M_γ have been carried out[35-37]. Currently, only purely empirical connections between these characteristics and mass of the fissioning system have been made[38]. However, we are now able to understand better the underlying fundamental relationships if we combine our data with known fragment yield information (Fig. 4). Here, we manage to relate two independent average quantities, the mass and the spin, for light, heavy and average fragment masses, and use our parametrisation to make predictions for other systems.

We also note that fission is a production mechanism used to study the structure of exotic nuclei[15,16]. Thus, understanding spin generation will allow determination of which excited nuclear states can be accessed.

Finally, outside the actinide region fragment-yield distributions evolve due to the changing influence of shell closures. For example, a transition from asymmetric to symmetric fission occurs for nuclei beyond ^{258}Fm[39]. In the newly-discovered region of β-delayed fission[40] around ^{180}Hg, the shell effects which drive the configuration at scission are not well understood. For fission regions which are less well explored, measurements of spin-sensitive γ ray data could yield valuable information on neck formation and the relevant shell closures involved.

Conclusion

A full theoretical description of nuclear fission requires incorporation of the intrinsic angular momentum generation mechanism. We have presented extensive experimental data on fragment spins in different systems from which it is now finally possible to discriminate between the many competing theoretical explanations of this mechanism. We show that fragment spins are uncorrelated, demonstrating the post-scission nature of the mechanism. Theoretical explanations based on pre-scission collective vibrations[4-8], post-scission Coulomb excitations[10], or coupling through fragment deformations are not supported by our data[9,11]. A parametrisation based on the expected occupation of spin states according to statistical theory well-describes the experimentally observed mass dependence of average spins.

Bibliography

[1] Wilhelmy, J.B., Cheifetz, E., Zared, R.C., Thompson, S. G., and Bowman, H.R., Angular Momentum of Primary Products Formed in the Spontaneous Fission of ^{252}Cf, Phys. Rev. C **5** 2041 (1972)

[2] Schmitt K-H. and Jurado, B., Review on the progress in nuclear fission—experimental methods and theoretical descriptions, Reports on Progress in Physics, **81** 10 (2018)

[3] Andreyev, A.N., Nishio, K., and Schmidt K.-H, Nuclear fission: a review of experimental advances and phenomenology, Rep. Prog. Phys. **81**, 016301 (2018)

[4] Rasmussen, J.O, Nörenberg, W., Mang, H.J, A model for calculating the angular momentum distribution of fission fragments, Nuclear Physics A136 465 (1969)

[5] Moretto, L.G., G. F. Peaslee, G.F., and Wozniak, G.J., Angular momentum bearing modes in fission, Nucl. Phys. A**502**, 453 (1989).

[6] Misicu, S., Săndulescu, A., Ter-Akopian, G.M., and Greiner, W., Angular momenta of even-even fragments in the neutronless fission of ^{252}Cf, Phys. Rev. C 60, 034613 (1999)

[7] Shneidman, T.M., Adamian, G.G., Antonenko, N.V., Ivanova, S.P, Jolos, R.V., and Scheid, W., Role of bending mode in generation of angular momentum of fission fragments, Phys. Rev. C 65 064302 (2002)

[8] Gönnenwein, F., Tsekhanovich, I., and Rubchenya, V., Angular Momentum of near-spherical fission fragments, Int. J. Mod. Phys. E 16, 410 (2007)

[9] Bonneau, L., Quentin, P., and Mikhailov, A.N., Scission configurations and their implication in fission-fragment angular momenta, Phys. Rev. C 75, 064313 (2007)

[10] Hoffman, M.M., Directional Correlation of Fission Fragments and Prompt Gamma Rays Associated With Thermal Neutron Fission, Phys. Rev. 133, B714 (1964)

[11] Mikhailov, I.N., and Quentin, P., On the spin of fission fragments, an orientation pumping mechanism, Phys. Lett. B **462** 7 (1999)

[12] Bertsch, G.F., Kawano, T., and Robledo, L.M., Angular momentum of fission fragments, Phys. Rev. C99 034603 (2019)

[13] Rimpault, G., Bernard, D., Blanchet, D., Vaglio-Gaudard, C., Ravaux, S. and Santamarina, A., Needs of Accurate Prompt and Delayed γ-spectrum and Multiplicity for Nuclear Reactor Designs, Physics Procedia 31 3-12 (2012)

[14] Blanchet, D., Proc. M&C 2005, Int. Topical Meeting on Mathematics and Computation, Supercomputing, Reactor Physics and Nuclear and Biological Applications (2005)

[15] Dudouet, J. et al. 96Kr–Low-Z Boundary of the Island of Deformation at N=60, Phys. Rev. Lett. 118, 162501 (2017)

[16] Ha, J. et al., Shape evolution of neutron-rich 106,108,110Mo isotopes in the triaxial degree of freedom, Phys. Rev. C101 (2020) 044311

[17] Zagrebaev, V.I., Aritomo, Y., Itkis, M.G., Oganessian, Yu. Ts, and Ohta, M., Synthesis of superheavy nuclei: How accurately can we describe it and calculate the cross sections? Phys. Rev. C 65, 014607 (2001)

[18] Itkis, M.G., Vardaci, E., Itkis, I.M., Knyazhev, G.N., Kozulin, E.M., Fusion and fission of heavy and superheavy nuclei (experiment) Nuclear Physics A **944**, 204 (2015)

[19] Talou, P., Kawano, T., Stetcu, I., Lestone, J.P., McKigney, E. and Chadwick, M.B., Late-time emission of prompt fission γ rays, Phys. Rev. C **94**, 064613 (2016)

[20] Armbruster, P., Labus, H. , and Reichelt, K., Investigation on the Primary Spins of the 235U Fission Fragments, Zeitschrift für Naturforschung A26, 512 (1971)

[21] Pleasonton, F., Prompt gamma rays emitted in the thermal-neutron induced fission of 233U and 239Pu, Nuclear Physics A213 413 (1973)

[22] Glassel, P., Schmid-Fabian, R., Schwalm, D., 252Cf fission revisited - new insights into the fission process, Nuclear Physics A502 315 (1989)

[23] Naik, H., Dange, S. P., and Singh, R. J., Angular momentum of fission fragments in low energy fission of actinides, Phys. Rev. C**71** 014304 (2005)

[24] Abdelrahman, Y. et al, Average spins of primary fission fragments, Phys. Lett. B **199** 4 504 (1987)

[25] Boutoux, G., et al. Study of the surrogate-reaction method applied to neutron-induced capture cross sections. Phys. Lett. B **712** 319 (2012)

[26] Lebois, M., Wilson, J.N., et al., Development of a kinematically focused neutron source with the p(^{7}Li,n)^{7}Be inverse reaction. Nucl. Instrum. Meth. A 735 145 (2014)

[27] Wilson. J.N., Lebois, M., et al., The LICORNE Neutron Source and Measurements of Prompt γ-rays Emitted in Fission, Phys. Proc. 64, 107 (2015)

[28] Lebois, M., Jovančević, N., Thisse, D., Canavan, R., Étasse, D., Rudigier, M., Wilson, J.N., The ν-Ball spectrometer, Nuclear Instrumentation and Methods in Physics Research, **960** 163580 (2020)

[29] Gaudefroy, L., et al. Impact of Coriolis mixing on a two-quasi-neutron isomer in ^{164}Gd and other N=100 isotones, Phys. Rev. C 97, 064317 (2018)

[30] Brosa, U., Grossmann, S., Müller, A., Nuclear scission, Physics reports **197**, p167 (1990)

[31] Franke-Arnold, S., Barnett, S.M., Leach, J., Courtial, J., Padgett, M., Uncertainty principle for angular position and angular momentum, New journal of physics, 6 103 (2004)

[32] Terrell, J., Neutron yields from individual fission fragments. Physical Review **127** 3 880 (1962)

[33] Göök, A., Hambsch, F. and Vidali, M., Prompt neutron multiplicity in correlation with fragments from spontaneous fission of ^{252}Cf, Phys. Rev. C **90** 064611 (2014)

[34] Bethe, H. A., An Attempt to Calculate the Number of Energy Levels of a Heavy Nucleus, Phys. Rev. 50, 332 (1936)

[35] Oberstedt, A. et al., Improved values for the characteristics of prompt-fission γ-ray spectra from the reaction ^{235}U(n_{th},f), Phys. Rev. C 87, 051602(R) (2013)

[36] Chyzh, A. et al., Systematics of prompt γ-ray emission in fission Phys. Rev. C 87, 034620 (2013)

[37] Qi, L., et al., Statistical study of the prompt-fission γ-ray spectrum for ^{238}U(n, f) in the fast-neutron region, Phys. Rev. C 98, 014612 (2018)

[38] Valentine, T.E., Evaluation of prompt fission gamma rays for use in simulating nuclear safeguard measurements. Oak Ridge National Laboratory Report, TM-1999/300 (2001)

[39] Flynn, K.F. et al., Distribution of Mass in the Spontaneous Fission of ^{256}Fm, Phys. Rev. C 5, 1725 (1972)

[40] Andreyev, A., et al. New Type of Asymmetric Fission in Proton-Rich Nuclei, Phys. Rev. Lett. 105, 252502 (2010)

Fig. 1 | Dependence of average spin on fragment mass. Average spins extracted for even-even nuclei produced in fast-neutron induced fission of ^{232}Th, ^{238}U and spontaneous fission of ^{252}Cf are presented along with statistical uncertainties. Single-parameter fits to the data are shown in black lines. The fitting parametrisation developed to explain the angular momentum generation mechanism is presented in the discussion section.

Fig. 2 | Correlation between fragment spins. Correlations between fragment and partner spins for the six most strongly populated fragments in the ^{238}U(n,f) reaction with associated statistical uncertainties. Weighted linear fits to the data points for each nucleus are shown. The fitted slopes are compared to the expected slopes for the spin mechanisms (a) pre-scission with correlated spins or (b) post-scission with uncorrelated spins in the inset. The blue band (a) was determined from Monte-Carlo simulations of the de-correlating effects of the neutrons and statistical γ rays (see methods and extended data Fig.3).

Fig. 3 | Schematic diagram of post-scission angular momentum generation. Independent torques for different scission configurations are shown with neck nucleons displayed in green. The straight black arrows illustrate sizes and example directions of the linear momentum vectors which generate the associated angular momenta. The corresponding positions on the saw-tooth distribution of the resulting average spins are shown on the right.

Fig. 4 | Relationship between average fragment spins and average masses. Fragment yield-averaged data with statistical uncertainties are shown. Left Panel: Data are compared to predictions from the parametrisation for the three fissioning systems, with light peak (L), heavy peak (H) and average for the system (A) marked. Right panel: The same data are plotted as a function of the average fragment mass with the black lines showing predictions for other systems from the parametrisation. Purple diamonds show specific predictions for the major fissile isotopes, ^{233,235}U, ^{239}Pu and in addition, ^{245}Cm.

Methods

Experimental Setup Samples of ^{238}U (81 g) and ^{232}Th (129 g) were irradiated with a pulsed neutron beam from the LICORNE neutron source (400 ns period) in the centre of the ν-Ball spectrometer for total acquisition times of 216 hours and 450 hours, respectively. The average neutron energy that provoked fission was 1.9 MeV. Triggerless data from the 184 detectors in the ν-Ball array were written to disk at high data rates of typically between 1 and 3 million γ-ray hits per second, and processed later offline. Each detected γ-ray energy was associated with a unique 64-bit time stamp accurate to sub-nanosecond precision, thanks to the state-of-the-art FASTER digitisation system[41]. γ-ray coincidence events were identified offline with a minimum trigger condition defined as at least two unsuppressed high-resolution Germanium (Ge) detectors and at least one other detector module (BGO or $LaBr_3$) firing within a short 80 ns time window. These events were subsequently sorted into two- and three-dimensional histograms for further offline analysis. An additional data set was gathered from the ^{252}Cf spontaneous fission source inside an ionisation chamber[29] placed in the centre of the ν-Ball array for 52 hours. With this latter setup, one fragment was detected in-flight, while the other fragment was stopped in the backing of the sample.

Data Analysis Examples of γ-ray coincidence spectra are shown in Extended Data Fig. 1 and Extended Fig. 2. which support the main findings of the article. The lack of dependence of the ^{140}Xe intensity pattern on the fissioning system is shown in Extended Data Fig. 1, and the lack correlation between ^{140}Xe and ^{96}Sr fragment intensity patterns are shown in Extended Data Fig. 2.

The main experimental data on average spins after neutron emission presented in this article rely on a method which was initially developed at Manchester University in the late 1980's and described fully in ref [24]. It will henceforth be referred to as the Manchester Spin Method (MSM).

The MSM relies on measuring the relative intensity of every resolvable γ-ray transition for a given nucleus populated in the reaction of interest. At each level with spin I, the intensity difference between the observed ingoing and outgoing transitions is computed. This difference is defined as the direct side-feeding, S, of the state. The average spin populated is therefore the side-feeding-weighted average of the level spins over all n levels, $< I > = \sum_{i=1..n} I_i S_i / \sum_{i=1..n} S_i$. A further small correction in the result is necessary to account for the angular momentum carried away by the statistical transitions, which depends on the reaction and is deduced from γ-ray decay models at around 1 extra unit in the case of fission.
The MSM condenses all the available γ-ray intensity and coincidence data for a given nucleus into a single number, the average spin after neutron emission. It is thus a powerful experimental tool to study angular momentum effects in nuclear reactions. The method measures a cumulative intensity flow through many different excited states, all of which will eventually reach the ground state. There is a redundancy in the measured information and the method has a low sensitivity to individual γ-ray intensities (i.e. a large perturbation in the intensity value of any particular γ ray from the decay pattern has a small impact on the result). For example, the inclusion or exclusion of the intensities of transitions from states other than those with the lowest energy for a given spin (so-called yrast states) levels in the calculation is seen to have very little impact on the result (see the section on "non-inclusion of weak transitions"). If the yrast sequence of transitions is observed, then an average spin can be extracted from the data.

We note that the first experiment where the MSM was applied used only 12 Compton suppressed small-volume Ge detectors to study heavy-ion induced fission. In our work, we measure neutron-induced fission with a high-performance third-generation γ-ray spectrometer with 106 large-volume, Compton Suppressed Ge crystals and state-of-the-art, triggerless signal digitisation technology.

Application of the MSM to ν-Ball data In the present work on nuclear fission, we measured the average spin in around 30 even-even nuclei in each system (see Extended Data Tables 1, 2 and 3). Even-even nuclei have relatively simple, well-known, decay schemes and are generally much easier to study. Even-odd and odd-odd isotopes often have highly fragmented decay patterns with many low-energy transitions, which are difficult to detect. The presence of a neutron beam pulsation, or in the case of the spontaneously fissioning ^{252}Cf(SF), direct detection of one of the fission fragments in the ionisation chamber is crucial for distinguishing between γ rays from prompt fission and those from subsequent fragment β decays. This latter source of γ rays is usually associated with low multiplicity events (M_γ ~ 2-3), but for certain isotopes can be comparable to that of fission. Emission of γ rays after β decays is uncorrelated in time, whereas 95% of prompt fission γ rays are emitted within a few nanoseconds of the beam pulse or fission event. Without the beam pulsation, γ rays from β-decay and prompt fission events are difficult to discriminate. This can lead to difficulties in extracting fragment average spin from intensity measurements, since population of nuclei via both processes occurs. The closer to stability the nucleus, the more of a problem this represents. ^{252}Cf (SF) has been extensively studied by spectroscopists over the last twenty years[42,43] but mostly from data sets without direct fission fragment detection, where the primary focus has been on extending knowledge on the nuclear structure of exotic neutron-rich nuclei. Spin effects in ^{252}Cf(SF) may have been difficult to study without an ability to discriminate γ rays from fission and β-decay.

γ-ray coincidence data and efficiency calibrations Application of the MSM requires determination of the γ-ray full energy peak detection efficiency over a wide range of energy

100 keV - 5 MeV. Each of the three systems studied (^{232}Th, ^{238}U, ^{252}Cf) has its own unique efficiency curve due to different target/chamber geometries producing slightly different self-shielding effects at lower energies. These were determined by combining GEANT IV[44] simulations of the setup for the highest energy part (2 - 5 MeV), source measurements, and measurements from the fission coincidence data for the lowest energy part (100 - 500 keV). For the lowest part of the energy range, self-shielding effects in the massive ^{232}Th and ^{238}U targets are particularly important, and are difficult to simulate due to the complex, non-uniform distribution of fissions within these targets. The drop in efficiency below 200 keV is significant and is measured from the experimental data by gating on γ-ray yrast cascades in rotational nuclei (e.g. Ce and Mo) from above and measuring efficiency ratios for the transitions below. Uncertainties on these efficiencies are included in the data analysis for the measurement of γ-ray intensities and in the subsequent deduction of average spins after neutron emission.

Fitting procedures Global fits of many thousands of γ-ray coincidences were performed in two dimensional (2D) γ-γ coincidence matrices using the Radware software package[45]. Two dimensional analysis is essential to measure 4+ state side-feedings. Since many nuclei share similar transition energies, a global 2D fitting procedure is needed for accurate measurements of transition intensities. Odd-even and odd-odd nuclei also need to be included so that all the possible coincidences can be identified in a particular matrix slice or region. Level scheme information from the evaluated ENSDF libraries[46] containing level spins, excitation energies, transition energies and coincidence relationships, are used as the starting point for each nucleus. Peak width parameters are fixed from a pre-determined width calibration as a function of energy. The intensities, G_k, and energies of the observable transitions are then fitted simultaneously for all nuclei in a global fit with thousands of free parameters. Subsequent local fits for each nucleus are then performed to check convergence at the local level, with global parameters fixed and only local parameters free to vary. Global and local fits are then repeated iteratively until convergence is achieved. At each stage, Radware calculates a χ^2/degree of freedom which is used to verify and assure convergence for each nucleus. Additionally, Radware also allows for powerful visual comparisons between the fitted γ-ray coincidences and the experimental spectral data. This facilitates a large number of visual checks to be performed to assure the level scheme of each fragment is correctly fitted and the local fit has fully converged. Global fits serve only as second order corrections to fit properly the rare occurrences that one fragment contains a pair of transitions of similar energies to those in another fragment.

To process the results of the fitting procedure and to extract side-feedings and average spins for each nucleus, new software has been developed which operates on the fitted intensity and peak position output from Radware. The side-feeding S_i of each level is computed from the sum of all observable transition intensities, G_k, feeding in and out of each level.

The software checks the level scheme transition intensities for self-consistency. Negative side-feedings are unphysical and if detected may signal a potential problem with the fitting of transitions feeding in or out of a particular level. Finally, the code computes the average spin for each nucleus studied by combining the level spins I_i and the side-feeding S_i information $< I > = \sum_{i=1..n} I_i S_i / \sum_{i=1..n} S_i$.

Propagation of uncertainties and variance-covariance The computed statistical uncertainty on the intensity of a particular transition is dependent on statistical variations in the number of counts at coincidence peak positions in two dimensions. A relative uncertainty in the level of background of 5% is assumed along with a typical relative uncertainty in the detection efficiency of 3%. For transitions below 200 keV the relative uncertainty on the detection efficiency rises to 20% due to the significant drop in detection efficiency over this energy range.

To determine the uncertainties on the extracted average spins $<I>$, the uncertainties on the fitted experimental intensity data are propagated through the MSM. However, the intensities, G_k, and side-feedings, S_i, are not necessarily independent and correlations may exist between these parameters. Therefore, correct mathematical treatment of error propagation requires the incorporation of potential correlated sources of uncertainty. Analysis of variances and covariances are needed first for the intensities, G_k, to determine the uncertainties on the S_i and then for the side-feedings to determine the error on average spin $\sigma_{<I>}$in the following way

$$\sigma^2_{<I>} = \sum_{i=1..n} I_i^2\, \sigma^2(S_i) + \sum_{i=1..n} \sum_{j=1..n\ (i\neq j)} I_i^2 I_j^2\, cov(S_i, S_j)$$

where $cov(S_i,S_j)$ is the matrix of covariances.

As the ν-Ball detector array uses Ge detectors which have an excellent resolution, a high detector granularity, and a "low" overall efficiency (~5%), the vast majority of covariances between intensity parameters are zero. Within the same level scheme, the off-diagonal elements of the variance-covariance matrix are typically (< 0.05), hence the independence of the G_k's can be considered a realistic assumption. However, the same cannot be said of the S_i's which are computed from intensity differences between neighbouring transitions in the scheme. The adjacent side-feedings S_i are thus strongly correlated with each other giving rise to both large negative and positive off-diagonal elements in the corresponding covariance matrix (~|0.4-0.8|). To perform the propagation requires the computation of a covariance matrix $cov(S_i,S_j)$ for each data point of $<I>$. This is complex and laborious, and given the number of data points, each one derived from a separate level scheme with its own unique set of coincidence relationships, this procedure for uncertainty calculation is challenging.

A more practical method for obtaining good estimates of the statistical errors associated with each average $<I>$ is to fit the side-feeding distribution as Extended Data Fig. 4 and use the resulting uncertainty on the fitted average of this distribution. Here, there may be some small dependence of the uncertainty on the exact form of the fitting function chosen. This procedure for uncertainty estimation yields uncertainties comparable in size to the application of variance-covariance analysis.

Using the example of the ^{238}U(n,f) coincidence data, the observable intensities vary from the strong, e.g. ^{140}Xe $4^+ \rightarrow 2^+$ at 3.42(11)% of the total yield, to the very weak $14^+ \rightarrow 12^+$ in ^{150}Ce at 0.024(16)% of the total yield. The median relative statistical uncertainties on transition intensities from the global fit is 13%, and for level side-feedings is 24%. This gives rise to a typical relative average spin uncertainty of around 5%.

Sensitivity of the MSM

The level of accuracy, or sensitivity, of the MSM is an important question. To what extent are side-feeding distributions measured at or near the yrast line distorted by local quirks of the nuclear structure, leading to non-statistical inaccuracies in the average spin measurement for a particular nucleus? There are two empirical answers to this question: The first is addressed by the sensitivity analysis of the method to the inclusion or exclusion of non-yrast states (r.m.s average difference 5.9%). This implies a potential variation in the sensitivity of the method in the range of 0.3-0.6 ħ due to the degree of incompleteness of the spectroscopic information.

A second estimation of the sensitivity, or accuracy of the MSM can be obtained from analysis of the non-statistical variations of the data points around the fitted trends. The correlation coefficients obtained from the fits (see Extended Data Table 4) have values of typically R^2=0.85, implying that ~15% of the variation is not accounted for by the fit. The statistical uncertainties account for an additional ~5% of the variation (e.g. r.m.s average of 5.5% for the ^{238}U(n,f) reaction). Hence ~10% of the variation of the variation remains unaccounted for. This can originate from three sources: second order physics effects not included in the smooth parametrisation, local spin miss-assignments/errors in the literature level scheme information, and local biases due to peculiarities of the local nuclear structure. The trend is measured over a range of approximately 4-10 ħ and hence we deduce that in the worst case, the sensitivity of the method is in the range 0.4 -1.0 ħ.

Methods: Corrections applied in the MSM

The MSM involves some further small corrections due to possible residual coincidences from β decay, for the side feeding of the first 2^+ state, for the presence of isomeric states, and finally for statistical transitions from the continuum of unresolved non-yrast states. The correction methods are outlined in the following subsections, followed by a description of how a transition intensity can be deduced indirectly, if it cannot be obtained directly or accurately fitted.

Beta decay The experimental conditions were arranged to strongly suppress β decay, achieved by tagging one fission fragment in the ionisation chamber for ^{252}Cf(SF) and by pulsation of the neutron beam with 400 ns period in the cases of ^{232}Th(n,f) and ^{238}U(n,f). Additional corrections were employed to remove any residual γ-ray coincidences from β decay in the neutron-induced reaction data by subtracting an uncorrelated background. Background coincidence matrices were created using a pre-prompt trigger window 200 ns before the beam pulse of exactly the same size as the prompt window (80 ns). Typically, the correction applied is very small, since these matrices contained only 1-2% of the total counts of the prompt matrices, yet these subtractions are potentially important for the fragments closest to stability towards the end of the β-decay chains in fission (e.g. ^{98}Zr, ^{142}Ba, etc.). γ-ray coincidences from these nuclei will have larger components produced by this unwanted population process. If the correction is not applied this could lead to underestimates of the average spin in these particular nuclei due to the presence of unwanted β-decay population pathways at lower spins.

Determination of the side-feeding of the first 2^+ state The side feeding of the first excited state (2^+ in almost all even-even nuclei) cannot be measured directly from the γ-γ coincidences of a particular nucleus. However, as noted in the original MSM paper[29], it is possible to determine this side-feeding by selecting a strong transition in a partner fragment. The intensity ratio of the transition from the first excited state to the ground state, and the transition(s) feeding the first excited state can then be measured from the resulting spectrum and uncertainty determined. This ratio, labelled $G_{(2/4)}$ and shown in Extended Data, Tables 1 and 2, is always greater than or equal to unity, since negative side-feedings are unphysical.

These ratios cannot be determined directly for all of the fragments studied either because they and their partners are weakly populated, or in some cases the transition energy is a doublet common to both fragment and partner, or two neighbouring partners. We therefore fit the trends of $G_{(2/4)}$ ratios as a function of fragment mass in the light and heavy peaks for both the ^{232}Th and ^{238}U, and use the fitted values with appropriate uncertainties. The $G_{(2/4)}$ ratios for the light peak show a gradual trend towards unity at the highest masses. However, the $G_{(2/4)}$ ratio in the heavy peak is initially high (around 2.5) near the doubly-magic Sn shell closure and decreases rapidly towards unity with increasing mass. In the most extreme case, the side-feeding of the 2^+ state in ^{132}Sn populated in the ^{238}U(n,f) reaction accounts for some 60% of the total side-feeding intensity. This phenomenon may thus account for some of the observed anomaly at Z=50 when using the γ-ray coincidence method to determine fission yields[47].

For the ^{252}Cf(SF) system it is not possible to deduce the 2^+ side-feedings from gating on the partner fragments since the partner fragment decays in-flight, so its transitions are Doppler broadened. In the case of ^{252}Cf(SF) we use $G_{(2/4)}$ ratio values deduced from the fits to the ^{238}U(n,f) data. The ^{232}Th(n,f) $G_{(2/4)}$ ratios show similar variations with mass, but we assume the ^{238}U(n,f) trends provide better estimates. This is preferable to assuming 2^+ state side-feeding values of zero for ^{252}Cf(SF), since it allows a better comparison of average spins in all three systems, but may necessarily introduce some small systematic bias.

Statistical transitions The statistical side feeding transitions will also carry away a small quantity of angular momentum. In the original MSM paper calculations were used to estimate the average number of statistical transitions (2.5) and average angular momentum per transition (0.4 units)[48]. Here, we use these same values to facilitate comparison of results. These do not impact the shape of the observed saw-tooth distributions but will instead just shift them globally up or down in spin.

Isomeric states and delayed transitions Calculating the average spin for a nucleus with a strongly populated isomer requires an additional step in the analysis. For isomeric transitions with lifetimes in the ns - μs range, the γ-ray decay below the isomer can occur outside the trigger window and thus the γ-rays and their coincidences with states above the isomer are not observed, leading to an underestimate of the average spin if no correction is applied. The correction for ^{252}Cf(SF) data is very simple, since we can just increase the size of the prompt window from 100 ns to 4 μs. This results in an increase in the average spin of the most affected nuclei, ^{132}Sn and ^{134}Te, of 12% and 14% respectively. No other nuclei show statistically significant increases in the deduced average spin for an extended coincidence window. Applying corrections for isomers in the ^{232}Th(n,f) and ^{238}U(n,f) data sets is more difficult. The prompt window is increased from 80 ns to 400 ns, and the corresponding increase in spin for these key isomeric nuclei is measured. A further correction is then applied using an extrapolation to account for the missing isomeric coincidences beyond the 400 ns window.

For all three fissioning systems the nucleus ^{130}Sn presents a unique problem. A 10^+, 1.6 μs isomer decays to the 7^- state through an unobservable 96 keV transition and this 7^- state has a half-life of 1.7 m. Hence, there is missing intensity for this nucleus. We include ^{130}Sn in our data, but acknowledge the existence of a potential systematic error in the calculation of the average spin for this particular case. However, since the neighbouring ^{132}Sn also has a similar high spin isomer, and the inclusion or exclusion of these decays changes the average spin by only 12%, we assume that the systematic underestimate of average spin for ^{130}Sn will be smaller than the statistical uncertainties.

Redundancy and the indirect deduction of intensity information As mentioned previously, there is some redundancy in the γ-ray transition intensity since we measure a cumulative intensity flow. This redundancy can be exploited to recover missing intensity information in the rare case that it is necessary. A problem that can occur during a two-dimensional coincidence analysis is that occasionally, certain coincidences or transitions can be obscured by the presence of others if they are too close in energy. This generally presents more of a difficulty for a small number of weak transitions in nuclei with the lowest production yields. For example, there is a strong background of random 511 keV γ rays from electron-positron annihilation. For a nucleus that has a weak transition very close to this energy it is often impossible to measure its intensity directly due to the large statistical fluctuations present after subtraction of this dominating background.

If such doublets or multiplets are too close in energy to resolve by two-dimensional peak fitting, information on the intensity of the obscured transition can still be recovered from the intensity flows into and out its initial and final states. For the general case, the intensity, G, of a γ-ray transition between initial state A and final state B can never be smaller than the intensity balance into state A and never be larger than the intensity balance out of state B, since this would result in negative side-feedings for A or B, which is unphysical.

If G_{Ai} and G_{Ao} are the measured ingoing and outgoing intensities from state A, and G_{Bi} and G_{Bo} those for state B, then the intensity of the missing transition intensity, G_x, must obey the following relation $(G_{Ai}-G_{Ao}) \geq G_x \geq (G_{Bo}-G_{Bi})$. The best estimate of the intensity G_x is thus the average $((G_{Ai}-G_{Ao})+(G_{Bo}-G_{Bi}))/2$ of the upper and lower bound and implies the side-feedings of state A and state B are equal. The impact of deducing a γ-ray intensity on the average spin measured for a particular nucleus is not significant, since the measurement integrates the intensity information from many transitions and the deduced intensity is usually a very good estimate of the real intensity.

Methods: Potential sources of bias

The MSM has several sources of potential bias outlined in the following subsections:

Level schemes Since we are observing neutron-rich nuclei far from stability in these experiments, the level schemes in the literature (ENSDF databases) may have spin assignments of certain levels which are only tentative, and in some cases incorrect by 1 or 2 spin units. This may have a small impact on the average spin extracted for a particular nucleus. However, the main side-feeding branches usually occur at lower spins with the 2^+, 4^+ and 6^+ yrast levels accounting for a large fraction of the total side feeding intensity in most cases. These states are usually well measured with unequivocal spin assignments. Miss-assignment of the spins of certain states may either slightly lower or slightly raise the average spin deduced for a particular nucleus. However, the effect will be local, can occur in either direction, and will be confined to a particular nucleus. No global systematic effect is expected.

Ground state feeding The direct side-feeding of the ground state is impossible to measure using γ-ray spectroscopy. However, we can estimate it from an extrapolation of the spin distribution towards zero. Extended Data Fig. 4 shows how this extrapolation is performed from fits to the spin distribution associated with each data point. The extracted 0^+ feeding is given an appropriately large relative uncertainty. The 0^+ feeding is typically 3-5% of the total side-feeding intensity in most cases, but increases in the vicinity of closed-shell nuclei (up to 18% in the case of ^{132}Sn). The impact of this correction on the average spin values results in a slight lowering which is smaller than the statistical errors. However, for ^{132}Sn and its near neighbours with significant 0^+ feeding the average spin values drop more significantly by typically 0.3 ħ. Performing this correction has no impact on the conclusions.

Non-inclusion of weaker transitions A potential bias in extraction of average spin could occur as a function of the fragment yield. Nuclei which are more weakly populated in general, may have fewer observable transitions and levels available for inclusion in the weighted sum. However, we conclude that the MSM method is very insensitive with respect to the inclusion or exclusion of non-yrast levels. Provided transitions from levels in the yrast sequence are visible, a reliable extraction of average spin can be made. The non-observation of weak transitions at the top of the yrast sequence has little impact on the final result, since if the transitions are weak at this point, the side-feedings are also weak and contribute little to the result. To quantify this potential bias average spins in the 15 most strongly populated nuclei were recalculated after fitting only the yrast sequences and ignoring the presence of all other non-yrast states and transitions. The r.m.s. difference between the two sets of values was found to be 5.9%. The transition rates of statistical side-feeding transitions are orders of magnitude faster than the intra-yrast cascade transitions and this probably accounts for why the difference is small. Finally, if the measured average spins for all nuclei studied are plotted against fragment yields, the two quantities are seen to be almost entirely uncorrelated.

The trigger condition For the case of the ^{252}Cf(SF) the trigger condition was an anode signal of the ionisation chamber corresponding to detection of one fragments in flight, with the other stopped rapidly in the backing of the sample. This gives a clean, unambiguous signal that a fission has occurred. For the ^{232}Th(n,f) and ^{238}U(n,f) reactions the fission discrimination is less perfect. While the beam pulsation allows discarding of events which are uncorrelated in time, a minimum multiplicity condition is also used in the prompt trigger window. This is essential to discriminate fission from the complex background of other low-multiplicity processes which also occur during the beam pulse, such as inelastic scattering ^{238}U(n,n′), ^{27}Al(n,n′), ^{72,73,74,76}Ge(n,n′) , p(^{7}Li,^{7}Li′) Coulomb excitation of the primary beam, and the intrinsic activity of the targets. The intrinsic activity is a particular problem for the ^{232}Th target, as a fraction of its decay also occurs during the prompt beam pulse. Since the majority of γ-rays detected during the experiment come from these low-multiplicity processes, a minimum trigger condition of $M_\gamma >= 3$ is essential to preferentially select fission events. For the best discrimination the trigger condition should be placed at even higher multiplicities but we have deliberately kept it at 3 to minimise any potential trigger biases, even though this results in larger backgrounds. From the ^{252}Cf(SF) data it is possible to study the impact of the multiplicity trigger condition on the results. Raising the minimum trigger condition from ionisation chamber fission tag from a minimum multiplicity of two to three has no significant impact on the measured average spins. Effects are, however, observed at higher multiplicity conditions. A global increase in the average spin for all nuclei of around one spin unit is observed for an increase of around 4 units in detected multiplicity. This correlation is completely expected and gives further confidence in the key observation of this paper, namely the absence of spin correlations between fragment partners. The reason the slope of the correlation of average spin with detected multiplicity is not larger is mostly due to the imperfections in the ν-Ball calorimeter (68% efficiency for detecting a single γ ray at 1 MeV). An event of detected multiplicity (or fold) of 4 will thus have significant contributions from emitted multiplicities of 4, 5, 6, 7 and 8.

Derivation of the spin parametrisation from statistical theory The expected probability distribution, $P(I)$, of angular momenta, I, for an excited nucleus following the work of Hans Bethe[35] is:

$$P(I|\sigma^2) = \frac{2I+1}{2\sigma^2}\exp\left(-\frac{(I+½)^2}{2\sigma^2}\right)$$

where σ is known as a spin-cutoff parameter describing the breadth of this distribution. In the Fermi gas model, the spin cut-off parameter depends directly on the nuclear temperature, T, and is related to the excitation energy *Ex* and level density parameter, *a*.

$$T = \sqrt{\frac{E_x}{a}}$$

In this model, the spin cut-off parameter is then usually defined as the product of the rigid body moment of inertia, $\mathcal{I}_{rigid}$, and the temperature:

$$\sigma^2 = \mathcal{I}_{rigid}T$$

where for a spheroidal nucleus

$$\mathcal{I}_{rigid} = \frac{2}{5}A_F R^2$$

so $\mathcal{I}_{rigid} \propto A_F^{5/3}$. Using a level density parameter, *a* which is proportional to A_F the variation in the spin cut-off parameter with fragment mass can then be defined in the following way:

$$\sigma^2 \propto \sqrt{E_x}A_F^{7/6}$$

If we assume that the excitation energy of the fragment is proportional to the mass of the nucleons from the ruptured neck (i.e.$E_x \propto A_N$), we obtain this final parametrisation based on statistical theory which can be used to fit our average spin data in Fig. 1:

$$\langle I \rangle = cA_N^{1/4}A_F^{7/12}$$

where $\langle I \rangle \approx 1.15\sigma$. This smooth parametrisation of the mass dependence with only one free parameter can be used as a fitting function, analogous to the smooth fitting of nuclear mass variations with the Weissacker formula[49]. An extended theoretical description would also have additional local variations in $E_x(A_F)$, level density $a(A_F)$ and $\mathcal{I}_{rigid}(A_F)$ due to structure effects. However, the smooth functional dependence of $\langle I \rangle(A_F)$ captures the major ingredients of the variation.

Monte-Carlo code for correlated fragment spins For the data presented in Fig. 2, a dispersion propagation Monte-Carlo code was developed to understand what experimental slopes we would expect to see if the intrinsic angular momentum is generated by pre-scission mechanisms which produce correlated spins at scission (i.e. the precise width and location of case a. in the inset of Fig. 2). The emission of neutrons and statistical γ rays in each fragment will have a de-correlating effect on any spin measurements carried out at or near the yrast lines. The precise and only purpose of this code is to propagate realistic spin dispersions from scission to yrast simultaneously in both fragments due to emission of neutrons and statistical γ rays. It allows for (i) complete user control over the spin distribution parameters at scission, (ii) total control over the widths of the spin dispersions due to emission of both neutrons and γ rays, and (iii) the ability to output the resulting spin distribution observed at yrast when setting conditions on the spin distribution in the partner fragment.

Dispersions in spin due to neutron emission were taken as random +/- 0.5ħ per emitted neutron. To obtain statistical γ ray spin dispersions, the RAINIER code[50] was used to fully model the γ decay of several representative spherical and deformed fission fragments. Typical statistical γ ray spin dispersion distributions with a width of around +/-1.5ħ were then imported into our Monte-Carlo code.

The placement of different gating conditions at yrast on one fragment could then be simulated and the effect on the resulting spin distribution at yrast in the partner fragment could be determined (see Extended Data Fig. 3). A simulated experimental relationship between the gating condition at yrast in one fragment and the "measured" average spin in the other could then be probed and an "experimental" slope deduced. With these tools, a sensitivity analysis of the results to the parameters of the initial spin distribution and neutron/γ dispersions could be performed. The blue band in the inset of Fig. 2 for case a) gives a range of expected slopes (0.4-0.6) for fully correlated spins at scission for reasonable variations of these parameters. The conclusion is that statistical emission will slightly weaken any spin correlations present at scission but will not destroy them.

[Note also that similar experimental data exists for 1n partners. These are not shown in Fig. 2, which would have become much too cluttered. However, the results obtained are similar, with no significant slopes observed.]

An extension of this Monte-Carlo code to include the γ-ray spectrometer granularity and detection efficiency was also developed. Here, the concern was that demanding observation of a "high spin" state in one fragment might reduce the overall efficiency of detection due to potential biases towards higher multiplicity events involving many detectors. Since ν-Ball is a highly granular array (106 Ge separate Ge elements at large distances) this effect on the expected slopes proved to be completely negligible. However, for the case of very close-packed detector arrays (e.g. 6 clover detectors placed in cubic geometry) small negative slopes could arise due to such biases, suggesting an artificial anti-correlation between fragment spins.

Data Availability Statement

All data from which the conclusions of this paper are drawn are contained within this manuscript. All other data can be made available on reasonable request. The large quantities of raw data (approx. 120 Tb) are shared within the nu-ball collaboration on servers at the CNRS-IN2P3 Centre de Calcul in Lyon (https://cc.in2p3.fr). The ALTO facility of IJC laboratory has a transparent data management policy which complies with the relevant European directives on open data (https://ec.europa.eu/digital-single-market/en/european-legislation-reuse-public-sector-information). Raw data from the nu-ball collaboration will be made publicly available after a period of 5 years.

Code Availability Statement

All codes used in the data analysis can be made available on reasonable request.

[41] Etasse, D. et al, http://faster.in2p3.fr
[42] Hamilton J., et al., New Insights from Studies of Spontaneous Fission with Large Detector Arrays, Prog. Part. Nucl. Phys. Vol. 35, 635 (1995)

[43] Smith, A.G., et al., Spectroscopy of neutron-rich nuclei populated in the spontaneous fission of ^{252}Cf and ^{248}Cm, International Conference on Nuclear Structure, AIP Conf. Proc. 481, 1 283 (1999)

[44] Agostinelli, S., et al., GEANT IV - a simulation toolkit, Nucl. Instrum. Meth. A506, 250 (2003)

[45] Radford, D.C, Software for interactive graphical analysis of HPGe coincidence data sets, Nucl. Instrum. Meth. A361 297 (1995)

[46] Tuli, J.K, Evaluated nuclear structure data file. Nucl. Instrum. and Meth. in Phys. Res. A **369**, 2 506, (1996)

[47] Wilson, J.N., et al, Anomalies in the charge yields of fission fragments from the ^{238}U(n,f) reaction, Phys. Rev. Lett. 118, 222501 (2017)

[48] Pülhover, F., On the interpretation of evaporation residue mass distributions in heavy-ion induced fusion reactions, Nuclear Physics A**280** 1, 267 (1977)

[49] Weizsäcker, C. F., Zur Theorie der Kernmassen, Zeitschrift für Physik **96**, pages 431–458 (1935)

[50] Kirsch, L.E., Bernstein, L.A., RAINIER: A simulation tool for distributions of excited nuclear states and cascade fluctuations, Nuclear Instrumentation and Methods in Physics Research A, 892, 30 (2018)

[51] England, T.R. and Rider, B.F., Evaluation and compilation of fission product yields, Los Alamos Report, LA-UR-94-3106, ENDF-349 (1993)

Acknowledgements

We would like to thank the staff of the ALTO facility of IJC laboratory, Orsay, for providing the intense, precisely focussed ^{7}Li primary beams for very long periods that permitted the collection of large data sets with the ν-Ball spectrometer. We would also like to thank Witek Nazerewicz, Sven Åberg and Olivier Serot for helpful discussions of fission theory and for the latter two, assistance with the theoretical interpretation of our experimental results. We thank Gregoire Kessedijan for assistance with variance-covariance calculations.

Finally, we would like to thank the Gammapool international consortium for the loan of the Germanium clover detectors used to construct the spectrometer. This work was supported by the IN2P3/CNRS, France, the STFC UK Nuclear Data Network, the STFC (Grants No. ST/L005743/1 and No. ST/P005314) (PHR), the Marion Redfearn Trust (RCL). PHR, MB., ABo and PI acknowledge support from the UK Department of Business, Energy and Industrial Strategy (BEIS) via the National Measurement System. PK, PAS, and JW acknowledge the support from BMBF under grant NuSTAR.DA 05P15RDFN1. Funding from the HORIZON2020 program of the European Commission is acknowledged for Transnational Access to the ALTO facility under the Integrated Infrastructure Initiative, European Nuclear Science and Applications Research 2 (ENSAR2), Grant Agreement n° 654002. ABl, RBG and NW acknowledge support by the German Research Foundation (DFG Grant No. BL 1513/1-1). LF, VV, BG and VST acknowledge funding from the Spanish MINECO via FPA2015-65035-P and RTI2018-098868-B-I00. AA acknowledges funding Spanish MINECO via FPA2017-83946-C2-1-P and Ministerio de Ciencia e Innovacion grant PID2019-104714GB-C21. BF Acknowledges funding from the Polish National Science Centre under contracts No. 2014/14/M/ST2/00738 and No. 2013/08/M/ST2/00257. AK, KM, MP and EA acknowledge funding from the Polish National Science Centre under contracts No. UMO-

2019/33/N/ST2/03023, No. UMO-2020/36/T/ST2/00547 and No. UMO-2015/18/E/ST2/00217. DG acknowledges funding from the Norges Forskningsråd (Research Council of Norway) 263030. SL, GB, CP, SZ, LI, AG and SB acknowledge funding from the Italian Istituto Nazionale di Fisica Nucleare (INFN).

Author contributions

JNW participated in the construction of the ν-Ball spectrometer, contributed to the experimental data taking, organised the ν-Ball international collaboration, performed the analysis work presented here and wrote the main body of the paper.
DG helped with experimental and theoretical discussions, interpretation of results, manuscript preparation and resubmissions, calculations, plots and bibliography.
DT constructed the spectrometer, calibrated and optimized the spectrometer, kept the spectrometer running, contributed to the experimental data taking, performed data processing of the large quantities of triggerless data and helped distribute it to the collaboration.
ML organised the ν-Ball project, led the construction of the spectrometer, organised the experimental campaign, kept the spectrometer running, contributed to the experimental data taking and measured ν-Ball performances.
MR, NJ, RC, GH, RL and R-BG helped with the cabling of the ν-Ball spectrometer, supported the running of the spectrometer (filling with liquid nitrogen, monitoring detectors, etc), calibrated and optimised the spectrometer, contributed to the experimental data taking and performed offline data analysis.
DE developed and helped deploy the digital electronics used for the ν-Ball DAQ.
LG developed and deployed the ^{252}Cf ionisation chamber.
SO, CS, TK, PHR, ABl, NW, SL, BF, AA, MF, LF and others contributed to the theoretical discussions and interpretation of results.
SS helped with organisation, discussions and interpretation, bibliography and manuscript preparation.
FZ carried out fragment decay simulations using the RAINIER code.
All listed collaborators helped keep the experiment, the spectrometer and the data acquisition systems running over the period of 7 weeks during which the data were collected.

Competing Interests

The authors declare that they have no competing financial interests.

Author Information
Correspondence and requests for materials should be addressed to Jonathan Wilson (email: jonathan.wilson@ijclab.in2p3.fr).

Extended Data

Extended Data Figure Legends and Tables

Extended Data Fig 1. | γ-ray coincidence spectra for ^{140}Xe. Spectra are gated by the $2^+ \rightarrow 0^+$ transition for the three different fissioning systems studied in this work. The spins of states emitting the yrast sequence of transitions are marked. Strong γ rays from the binary partner fragments are indicated. γ rays from fragment partners in ^{252}Cf(SF), such as ^{112}Ru, were detected in flight and are thus not visible due to Doppler broadening. The ^{252}Cf (SF) spectrum has much fewer counts, but similar experimental sensitivity is achieved due to the elimination of significant backgrounds by direct detection of the fission fragment in the ionisation chamber with the γ-γ coincidences.

Extended Data Fig. 2 | Coincident γ-ray spectra from the ^{238}U(n,f) reaction gated on transitions from ^{140}Xe emitted from states of increasing spin. The fits to transitions decaying out of specific states of the partner nucleus ^{96}Sr are shown in red. The 492 keV transition from the 6+ state in ^{96}Sr in the 3rd panel is deduced from its neighbours rather than fitted, due to contamination. The intensity pattern is not observed to vary and the average spins in ^{96}Sr show no significant changes. The relationships between partner spins for several more nuclei are shown in Fig. 2.

Extended Data Fig. 3 | Monte Carlo simulations of events with correlated spins at scission. Placing conditions on the minimum spin at yrast of events in fragment 1 affects the yrast distributions of event spins in fragment 2.

Extended Data Fig. 4 | Examples of experimental spin distributions for a range of nuclei observed in the ^{238}U(n,f) reaction. Statistical uncertainties are shown. To eliminate the odd-even staggering effect and facilitate easy visualization, side-feedings of odd spins are redistributed equally between the two neighbouring even spins. The red curves are fits to the experimental data with one free parameter and are used to extract 0+ side-feedings via an iterative procedure.

Extended Data Table 1: ^{232}Th(n,f) average spin data. Fragment yields are taken from the ENDF.BVII evaluation.[51]

Extended Data Table 2: ^{238}U(n,f) average spin data. Fragment yields are taken from the ENDF.BVII evaluation.[51]

Extended Data Table 3: ^{252}Cf(SF) average spin data. Fragment yields are taken from the ENDF.BVII evaluation.[51]

Extended Data Table 4: Fit parameters for the light and heavy peak data for the three fissioning systems shown in Fig. 1. The fitting function is defined as $< I > = cA_N^{1/4} A_F^{7/12}$ with a single free parameter, *c*.

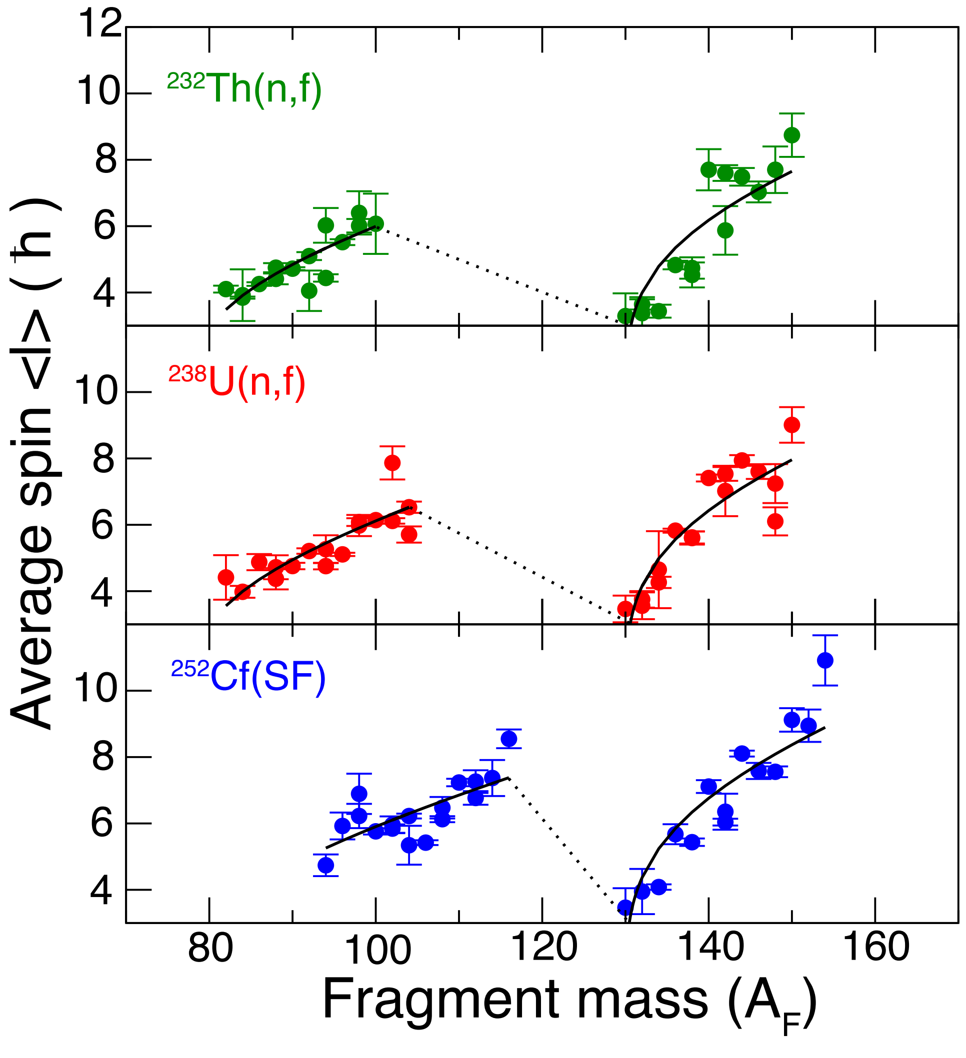

^{232}Th(n,f)
^{238}U(n,f)
^{252}Cf(SF)
Average spin <I> (ħ)
Fragment mass (A_F)
12
10
8
6
4
80
100
120
140
160

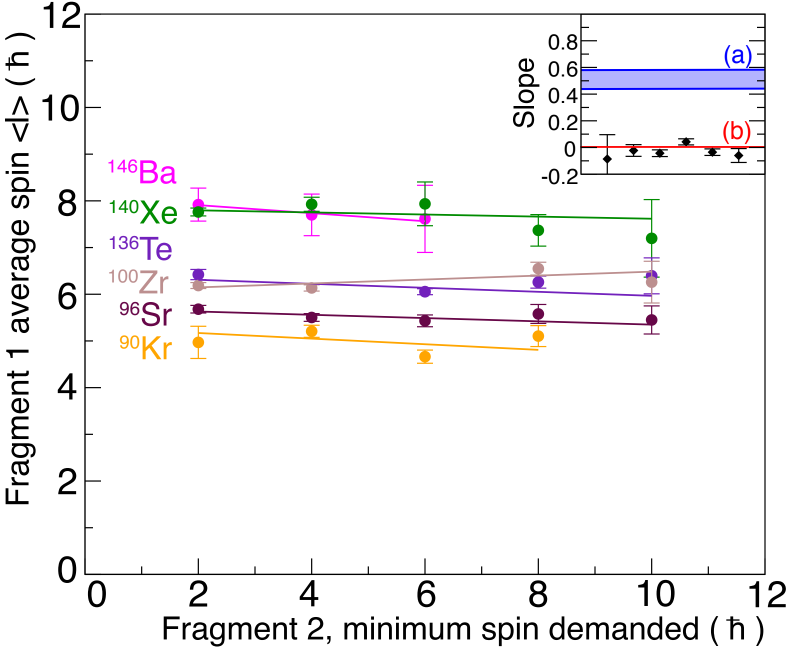

Fragment 1 average spin <I> (ħ)
Fragment 2, minimum spin demanded (ħ)
146Ba
140Xe
136Te
100Zr
96Sr
90Kr
Slope
(a)
(b)
0
2
4
6
8
10
12
0.8
0.6
0.4
0.2
-0.2

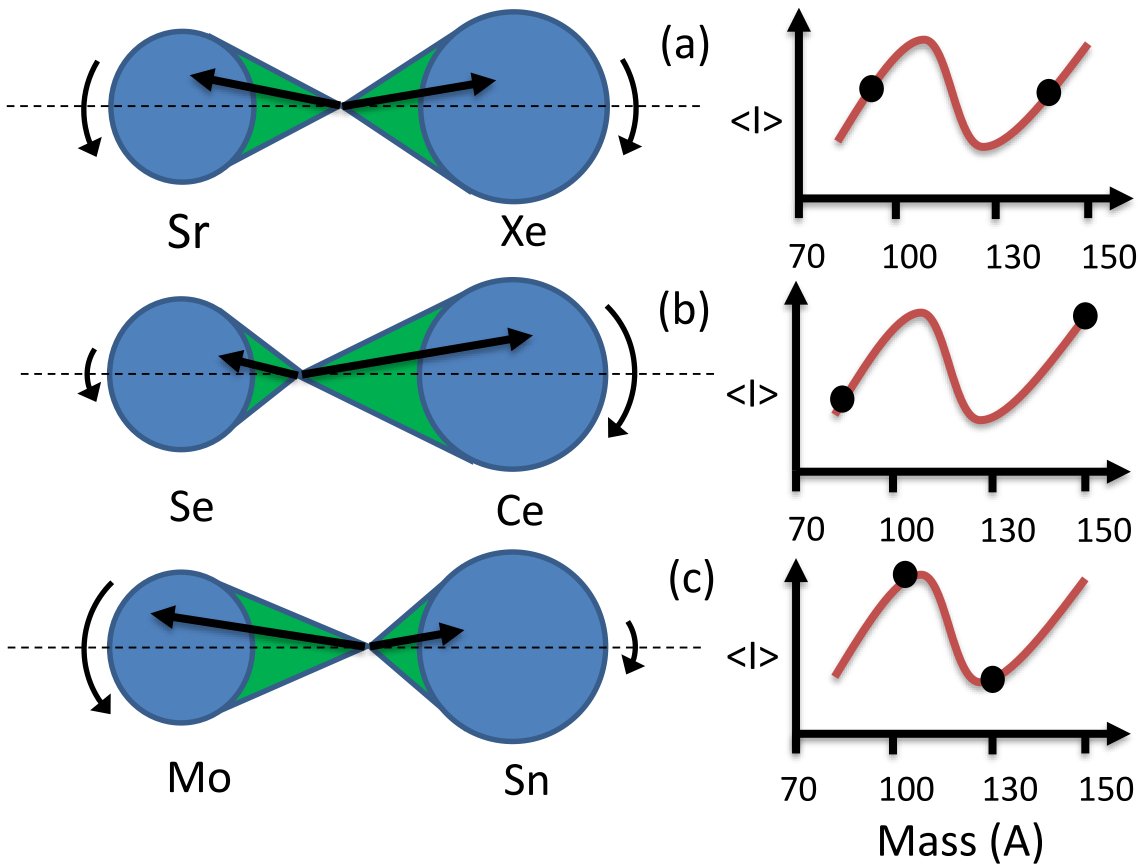

(a)
Sr
Xe
<I>
70
100
130
150
(b)
Se
Ce
<I>
70
100
130
150
(c)
Mo
Sn
<I>
70
100
130
150
Mass (A)

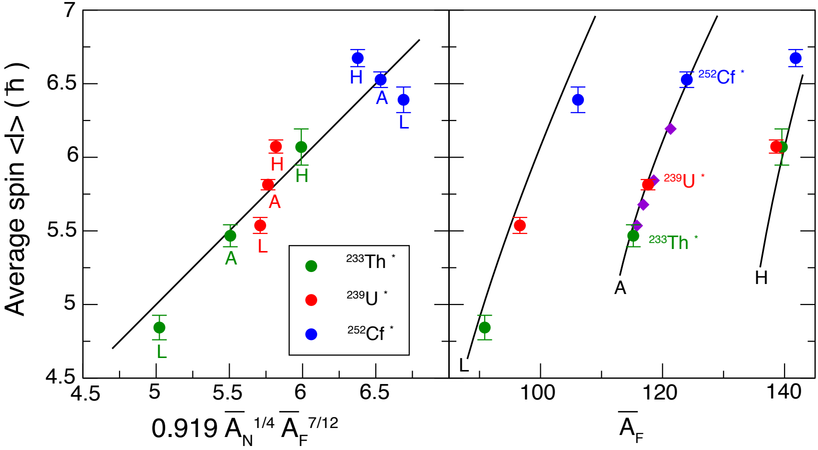

Average spin <I> (ħ)
7
6.5
6
5.5
5
4.5
5
5.5
6
6.5
0.919 $\overline{A}_N^{1/4}$ $\overline{A}_F^{7/12}$
H
A
L
H
A
L
H
A
L
^{233}Th *
^{239}U *
^{252}Cf *
100
120
140
$\overline{A}_F$
^{252}Cf *
^{239}U *
^{233}Th *
L
A
H